PERGAMON

International Journal of Heat and Mass Transfer 43 (2000) 867–884

International Journal of HEAT and MASS TRANSFER

www.elsevier.com/locate/ijhmt

Low turbulence natural convection in an air filled square cavity
Part II: the turbulence quantities

Y.S. Tian*, T.G. Karayiannis

School of Engineering System and Design, South Bank University, 103 Borough Road, London SE1 0AA, UK

Received 18 May 1998; received in revised form 4 June 1999

Abstract

An experimental study of two-dimensional low level turbulence natural convection in an air filled vertical square cavity was conducted at a *Ra* number of 1.58×10^9. Turbulence quantities including T'_{rms}, u'_{rms}, v'_{rms} and Reynolds stress are presented. The fluid flow was turbulent anisotropic wall shear flow. It was in the low turbulence region with a base frequency of about 0.1–0.2 Hz. The power spectral densities moved to higher frequency along the fluid flow. The temperature and velocity fluctuations were limited in the boundary layers along the solid walls and were not in Gaussian distribution. The results indicate that the temperature and the velocity components fluctuate separately.

Keywords: Natural convection; Cavity; Turbulence; Reynolds stress

1. Introduction

Turbulent natural convection is difficult to study and analyse because it is a multi-scale, coupled non-linear fluid flow problem. Fluid flow in rectangular cavities represents one of the simplest geometries with many applications in industry and nature. However, turbulent natural convection in vertical cavities is one of the most complicated fluid dynamic problems. Its complexity is characterised by the following factors: firstly, flow in a vertical cavity can include simultaneously laminar, transitional and turbulent regions when the Rayleigh number exceeds a critical value. Secondly, this boundary-like wall flow is basically anisotropic in its turbulent regions. Thirdly, due to the coupling of the boundary layer and the core region, neither the flow in the boundary layer nor the flow in the core region can be determined by the boundary conditions alone.

In Part I [1] the authors presented the mean temperature and velocity profiles including contour and vector plots. The flow structure was identified and the development and thickness of the thermal and momentum boundary layers were discussed. The work presented in [1] included local and mean heat transfer rates and the variations of the wall shear stress along the isothermal hot and cold walls. Comparison with earlier reports indicated reasonable agreement in the Nusselt number and velocity profile at mid-height. Differences were observed along the mid-width and when comparing change rates near the walls. In order to present a complete description of the low level turbulence flow in the cavity the turbulent fluid flow and

* Corresponding author. Tel.: +44-171-815-7600; fax: +44-171-815-7699.

E-mail address: karayitg@sbu.ac.uk (T.G. Karayiannis).

0017-9310/00/$ - see front matter
PII: S0017-9310(99)00200-8

Nomenclature

Ar_x	aspect ratio, $Ar_x = H/L$
Ar_z	aspect ratio for z-direction, $Ar_z = D/L$
D	depth of the cavity (m)
f	frequency (Hz)
F	flatness
g	gravitational acceleration (m/s^2)
H	height of the cavity (m)
k	turbulence kinetic energy (m^2/s^2)
L	width of the cavity (m)
Ra	Rayleigh number, $Ra = \frac{g\beta(T_h - T_c)L^3}{\alpha\nu}$
S	skewness
T	temperature (K)
u^*	friction velocity, $u^* = \sqrt{\frac{\tau_w}{\rho}}$ (m/s)
u, v, w	velocity component in x-, y-, and z-direction (m/s)
V_0	buoyancy velocity, $V_0 = \sqrt{g\beta\Delta TH}$ (m/s)
x	variable
x, y, z	coordinate
X, Y, Z	dimensionless coordinate
α	thermal diffusivity (m^2/s)
β	thermal expansion coefficient (1/K)
μ	dynamic viscosity (kg/m s)
ν	kinematic viscosity (m^2/s)
ρ	fluid density (kg/m^3)

Superscripts

-	time or integral average
$'$	fluctuation component
+	dimensionless parameter

Subscripts

b	bottom wall
c	cold wall
h	hot wall
rms	root mean square
t	top wall
w	wall
x	component along the width of the cavity
z	component along the depth of the cavity

thermal parameters and their values need to be measured, recorded and analysed. Such data for a 2D flow should include u'_{rms}, v'_{rms}, T'_{rms}, $\overline{u'v'}$, $\overline{u'T'}$, and $\overline{v'T'}$. These experimental values can then be compared along with the mean values with computational fluid dynamics (CFD) predictions. In particular, two additional terms are needed in the governing equations to describe turbulent natural convection, i.e. the Reynolds shear stress and the turbulent heat flux. The various turbulent models provide correlations for these two additional terms, therefore direct measurement of these quantities, although very difficult, is highly desirable.

In numerical studies, most researchers are now using the k–ε model. The wall law of the logarithmic velocity profile near the solid boundaries is very helpful in the modelling of forced convection. However, there is no suitable wall function for natural convection. The theoretical velocity profile in the fully developed turbulent boundary layer of natural convection, described by George and Capp [2], is not very useful because flow in cavities hardly reaches such conditions. As mentioned in Part I [1], the numerical results from various k–ε models are non-unique. A seemingly small difference in the models may be the source of inconsistencies in some values of the results. And none of the turbulent models can correctly predict whole velocity and temperature fields. The standard k–ε model predicts higher rate of change near the wall and the low Reynolds number k–ε model often gives laminar flow results. Generally, the k–ε models have difficulty accounting correctly for the anisotropic flow features. Some models predicted reasonable results of Nusselt number, temperature and velocity at mid-height but their ability to predict correct turbulent quantities is very poor. The Reynolds stress model is powerful but also considerably complicated due to the number of equations involved, for instance, a two dimensional problem needs 12 equations and many equation constants need to be validated using experimental data. An intermediate model that has much of the generality of the Reynolds stress model but also the economy of the two equation k–ε model is the algebraic heat flux model. Further work can be done in this direction following some success reported by Hanjalic and Vasic [3]. Large eddy simulation may not be suitable for the low turbulence flow in cavities due to the possible transitions from laminar to turbulent flow through the instability of small eddies [4]. Direct simulation is still too costly due to fine grid size, small time steps and large number of iterations. Even with that, sometimes unreasonable results were predicated, for example the double peak profile of turbulent kinetic energy reported by Paolucci [5] at the near wall region. In general, the discrepancy between the experimental and numerical results is obvious, especially for turbulent quantities.

Up to now, very limited experimental turbulence data were reported. Betts and co-workers [6,7] reported u' and v' results for a tall cavity ($Ar_x = 28.68$). Giel

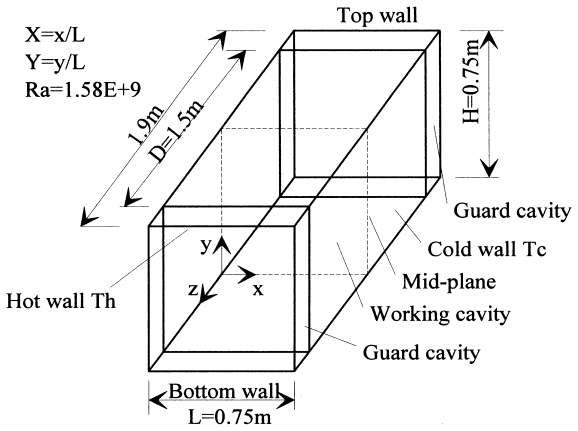

Fig. 1. 3D schematic view of the air filled cavity.

and Schmidt [8,9] measured v' and T' in a water filled high cavity ($Ar_x = 10$). Cheesewright and co-workers [10–14] built up a set of results including u', v', T', $\overline{u'v'}$, $\overline{u'T'}$, and $\overline{v'T'}$ for a cavity with $Ar_x = 5$. They used the measured mean values to calculate the Reynolds stress. Lankhorst [15] gave some v' results for a thin square cavity ($Ar_z = 0.1$). Mergui et al. [16] presented values of u', v', T' and $\overline{u'v'}$ for a shallow thin cavity ($Ar_x = 0.9$, $Ar_z = 0.3$). The results mentioned above featured strong asymmetry due to either heat losses [10–14] or limited aspect ratio in the depth direction [15,16].

Flow in cavities gets more confined near the wall as the Rayleigh number increases. The fluid velocity and temperature bear an abrupt change near the wall with a relative small absolute value. This feature gives a higher requirement on the instruments. For example, as seen in Part I [1], the velocity reaches its maximum of 0.225 m/s at a distance of 5–6 mm from the wall. The location of the thermocouples and the laser Doppler anemometer (LDA) probes must be known with high accuracy. The experimental cost needed to meet these requirements is considerably high. In addition, most previous experimental studies were carried either in high cavities or in thin square cavities. However, numerical researchers prefer 2D square cavities. Hence, accurate experimental results of turbulent quantities in square cavities which avoid some of the shortcomings of previous works are highly desired.

2. Experiment facility and procedure

As described in the Part I [1], a fully automatically controlled natural convection test rig has been carefully designed and constructed. A 3D schematic of the cavity is included in this paper, Fig. 1. The cavity was 0.75 m wide × 0.75 m high × 1.5 m deep giving two dimensional flow in the middle. Since a detailed description of the cavity, the experimental facility, the instrumentation and the procedure used was given in Part I [1] it will not be repeated here. A brief summary is given instead emphasising the accuracy of the instruments used and their ability to record turbulent quantities, i.e. fluctuation temperature and velocity.

A 2D LDA equipped with a burst spectrum analyser (BSA) was used in the velocity measurement. Incense smoke was used as seeding which lasted for more than 24 h. The velocity was measured on a non-uniform fine mesh. For every measuring location, either 20 K readings were taken (in the boundary layer) or the measurement taken for four minutes (in the core). The

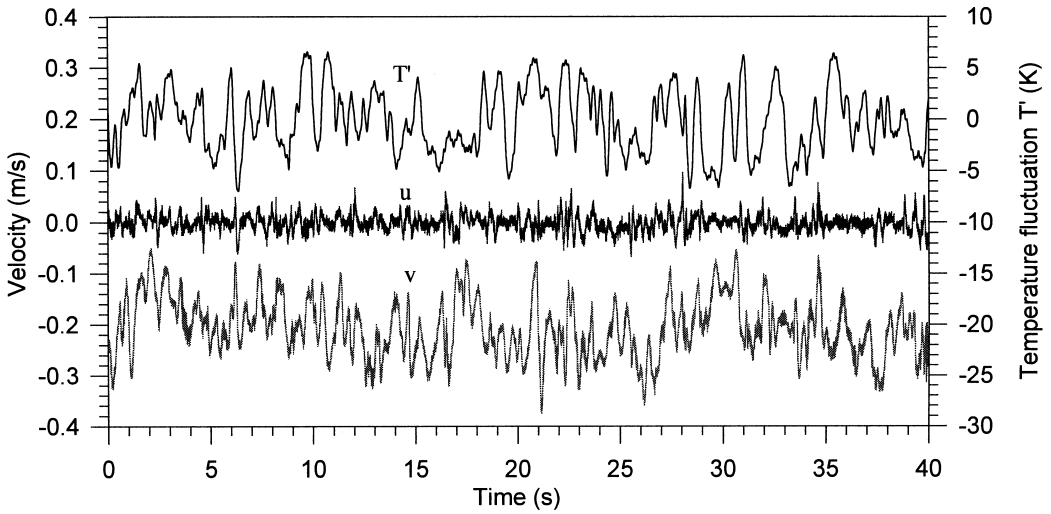

Fig. 2. Temperature and velocity signals at $Y = 0.5$, $X = 0.993$.

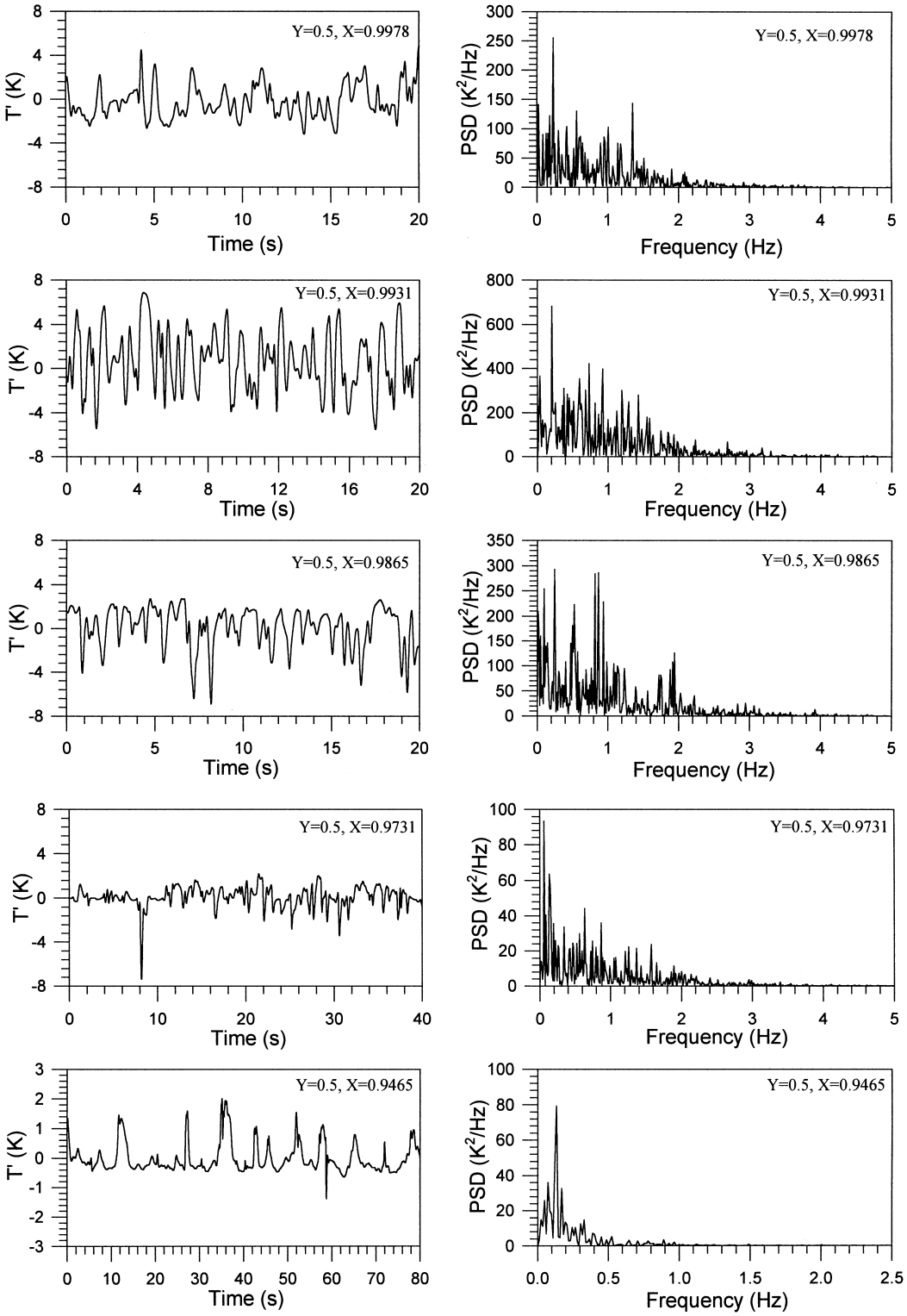

Fig. 3. Temperature fluctuation and its PSD distribution near the cold wall at $Y = 0.5$.

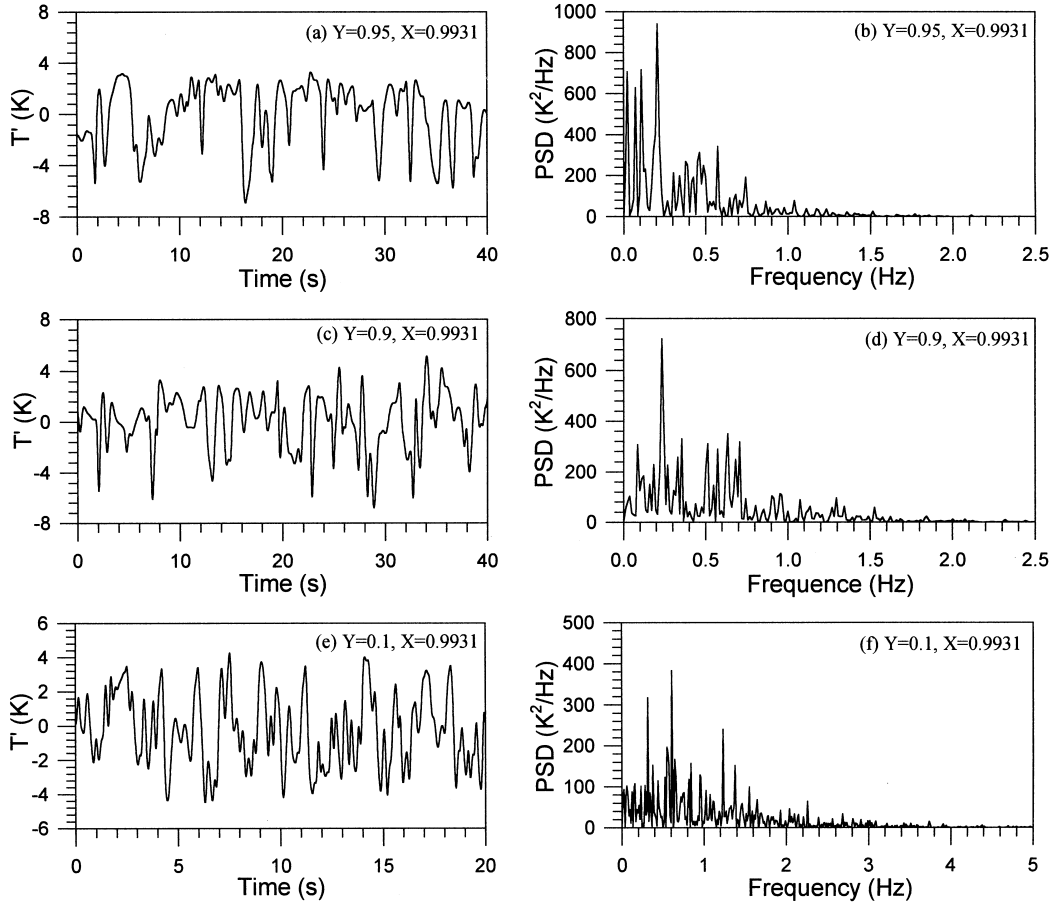

Fig. 4. Temperature fluctuation and its PSD at different heights near the cold wall.

highest data rate was more than 300 readings/second near the velocity peak and the lowest was 2 readings/second in the core area. The 3D traverse mechanism which carried the LDA probe was calibrated using a dial indicator (with 0.01 mm accuracy). The accuracy for the laser location was better than 0.1 mm. The two channels of the LDA were set to burst simultaneously so the Reynolds stress was measured. The technical difficulties in making accurate velocity measurements and the approaches adopted to overcome them were discussed by Tian et al. [17].

An E type thermocouple of diameter 25.4 μm with a response frequency of 20 Hz in still air was carried by a computer controlled 2D positional displacement device and was used to measure the air temperature in the cavity. The temperature was read by a 16 bit data logging card with low-pass filter at 50 Hz sample rate. 4096 readings were taken for each measurement. For every location, the measurement was made at least twice. If the difference between two measurements was less than 0.1 K (the average and the root mean square (rms) of the fluctuation), the second measurement was accepted and recorded. The accuracy of the thermocouple location was better than 0.2 mm and the temperature reading was true within 0.1 K. Special care was taken to insulate the thermocouple and the positional device from other parts of the rig so that the effects of electronic noise was reduced to a minimum (less than 0.1 K on the rms value), see Tian [18] for further details.

3. Experimental results

3.1. The time serials

The cavity was designed to produce low turbulence flow. The recorded temperature and velocity fluctuation signals are shown in Fig. 2. The T' rather than temperature, T, is shown in the figure for clarity ($T = \bar{T} + T'$). The horizontal (u) and vertical (v) velocity components were measured simultaneously. The

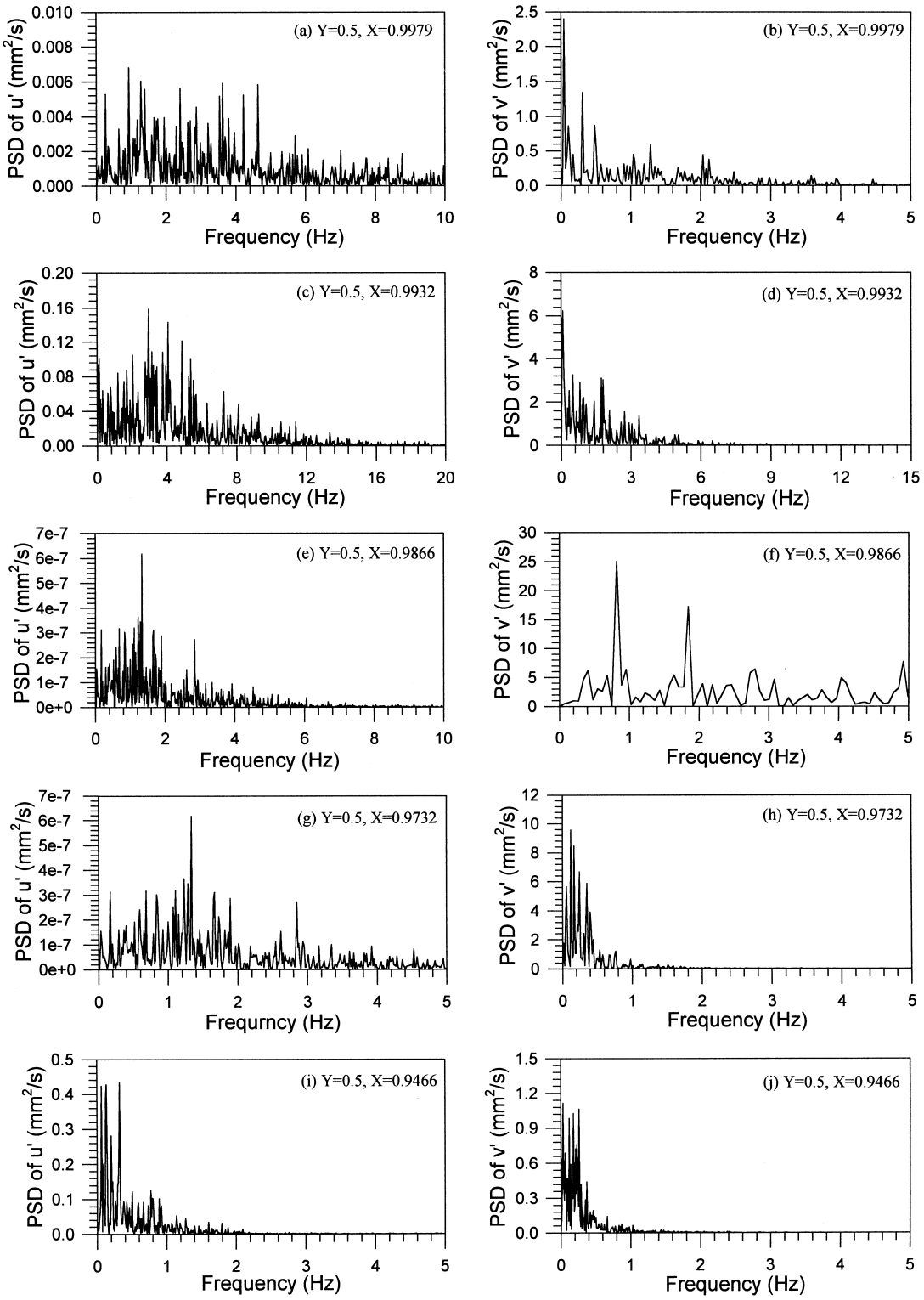

Fig. 5. PSD of the velocity fluctuation at mid-height near the cold wall.

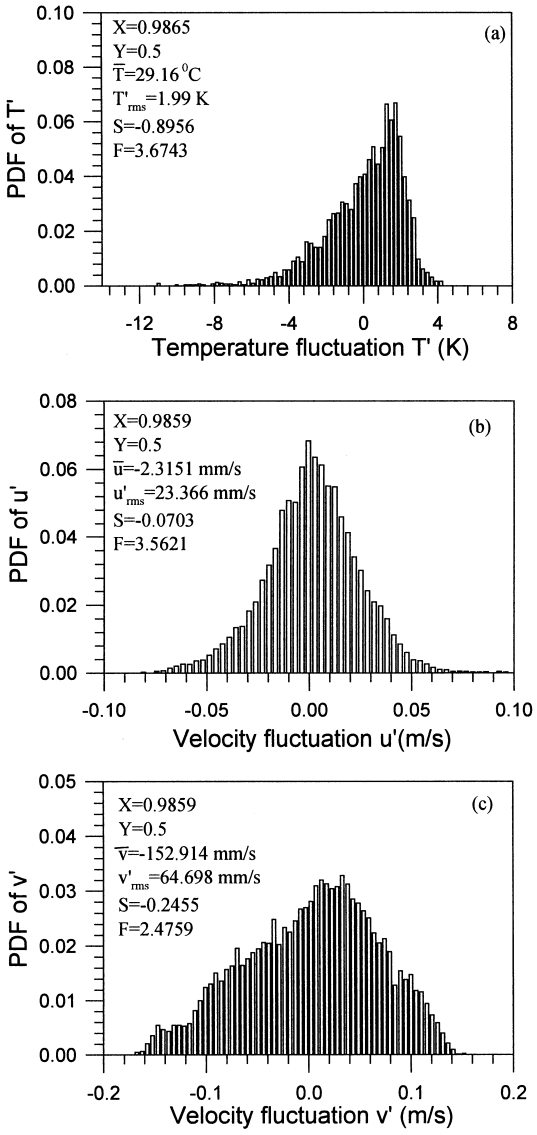

Fig. 6. PDF results at $Y = 0.5$.

temperature signals were measured separately. The low frequency seen in Fig. 2 indicates that the flow is in the low turbulence flow region in the boundary layer at mid-height. The theoretically estimated highest frequency based on the Kolmogorov scale and our maximum mean velocity is 60 Hz [18]. The time average velocity was very low and the maximum mean velocity was only 0.225 m/s. However, the velocity fluctuation can reach ± 0.16 m/s. The two velocity components fluctuated randomly (see also Section 3.2). Careful examination of the results reveals that there is no direct relation — phase or amplitude — between the two components. The total temperature difference in the cavity is 40 K ($T_h - T_c$), and the temperature fluctuation can reach ± 8 K. The fast Fourier transfer analysis was used to obtain the power spectral density (PSD) of the time serial results [18].

3.2. The power spectral density

The PSD is a function of frequency and expresses the distribution of power of the signal so it is also called power spectrum. It can be used to investigate the transition from laminar to turbulent flow [19]. The temperature fluctuation (T') at mid-height and different locations near the cold wall and the corresponding PSD as a function of frequency are shown in Fig. 3. One obvious feature is the spikes of the temperature signals. In the 4096 temperature points (in 81.92 s) of the time serial, the amplitudes of the spikes are not symmetric. This causes the time average temperature $\bar{T}$ and the rms value of the temperature fluctuation, T'_{rms}, to be unsteady. The shorter the time serial data, the more unsteady the $\bar{T}$ and T'_{rms} values appear. The results exhibit the discontinuity in frequency which is one of the features of a low turbulence flow. In laminar flow there is no physical parameter fluctuation and in a fully developed turbulent flow the fluctuation frequencies should be continuous. There are several peaks in the PSD distributions whose number depends on the turbulence intensity; more intense fluctuation results in more peaks. The PSD distribution has a very high peak at $f = 0.21$ Hz ($Y = 0.5$, $X = 0.9931$) near the maximum point of T'_{rms}. At the outer edge of the boundary layer, there is only one frequency (0.13 Hz) dominating the fluctuation ($Y = 0.5$, $X = 0.9465$). In the boundary layer, it seems that a base frequency of 0.12 Hz dominates the turbulence ($Y = 0.5$, $X = 0.9865$).

The experimental results at different heights, $Y = 0.95$, 0.9 and 0.1, are shown in Fig. 4. Careful examination of the T' and corresponding PSD results near the start of the boundary layer at the top cold corner, Fig. 4(a) and (b), indicates the existence of the doubling frequency relationship. However, its presence is not verified in all locations probably due to the small variable range of disturbances that lead to turbulence. As also seen in all PSD presented in Figs. 3 and 4, the base frequency of the temperature fluctuation is in the range of 0.10–0.15 Hz and the thermal turbulence is mostly concentrated in the low frequency regime, $f < 5$ Hz. A comparison of the results at the four different heights of Figs. 3 and 4 ($Y = 0.95$, 0.9, 0.5, 0.1 and $X = 0.9931$) clearly indicates the frequency shift. The turbulence intensity increases as the air flows from $Y = 0.9$ to 0.5 then $Y = 0.1$ near the cold wall, i.e. the turbulence frequency increases in the flow direction, and the PSD peaks move to higher frequencies. Laminar flow features were not found. The temperature distribution near the horizontal walls is

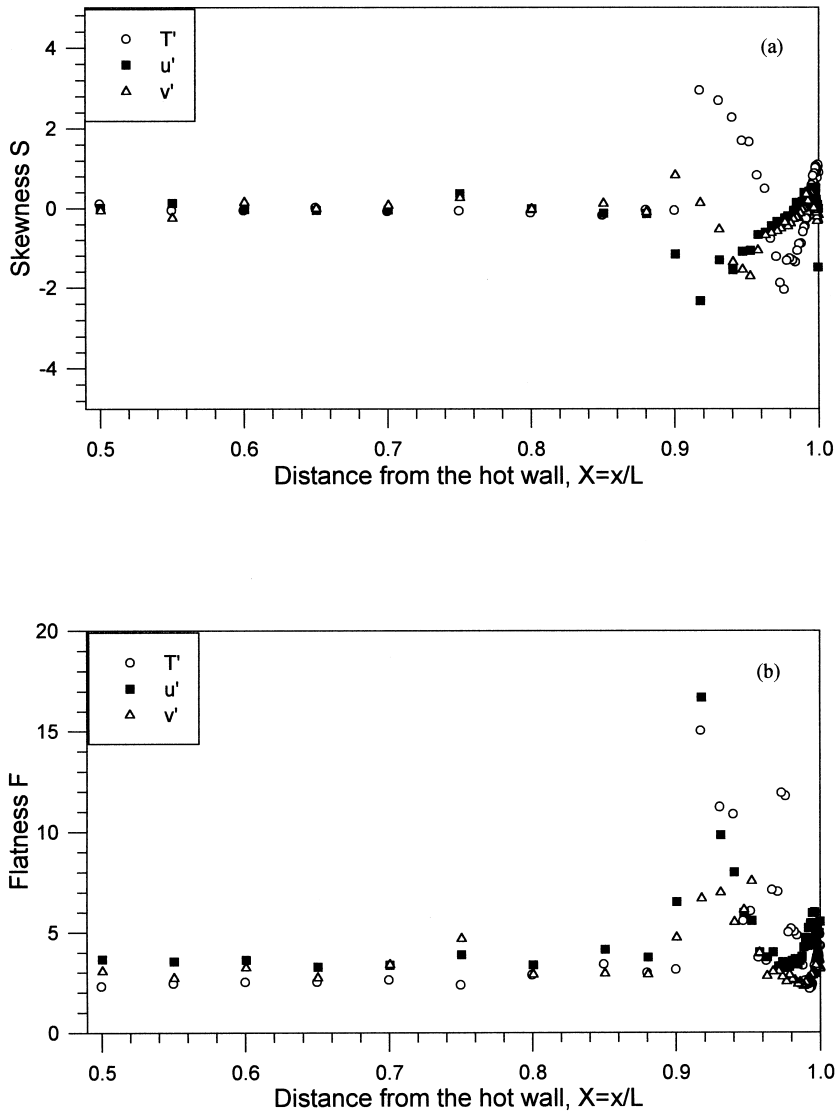

Fig. 7. Distribution of the skewness (a) and flatness (b) factors for T', u' and v' along the mid-height.

similar to the temperature distribution in the Rayleigh–Benard convection, i.e. the horizontal enclosure. This is due to the fact that, in our case, the horizontal walls are highly conductive. The Rayleigh–Benard instability is the dominant instability mechanism in the horizontal boundary layer.

The PSD results of the fluctuation of the two velocity components u' and v' at mid-height and different x locations near the cold wall are shown in Fig. 5. They also verify the low turbulence feature, i.e. many discontinuous peaks in the low frequency range. Careful examination of the results of Fig. 5 reveals that the peaks in the PSD results of u' and v' do not correspond to each other, i.e. the two components fluctuate randomly. There is no direct relation between the two fluctuating quantities, u' and v', either in power or in frequency. In Fig. 5(f), two peaks appear, at $f=$ 0.82 and 1.85 Hz. However, no other evidence shows frequency doubling, and no single value base frequency was found.

The fluid flow circulatory structure was presented in Part I [1] and as stated above, the flow along the horizontal walls possesses the Rayleigh–Benard instability. Turbulence is damped because of the change in flow direction as the flow approaches the vertical isothermal wall. However, the horizontal wall is not adiabatic so that the turbulence is not totally damped but 'passed on' to the vertical boundary layer where it is further

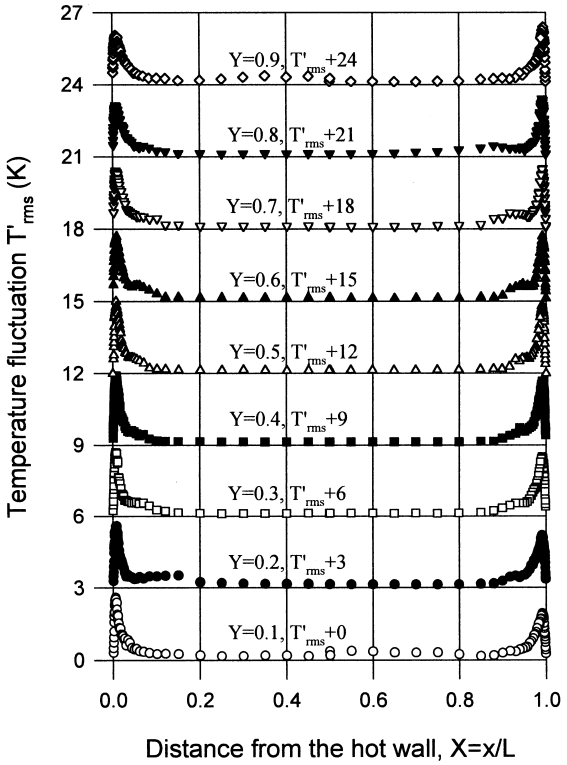

Fig. 8. Temperature fluctuation distribution, T'_{rms}, at different heights.

developed until the flow approaches the horizontal wall again. The fluid flow moves into the horizontal boundary layer with the Rayleigh–Benard instability only partially damped. The fluid flow in the vertical boundary layer inherits the partially damped turbulence and develops it from a lower frequency turbulent flow to a higher frequency turbulent flow. This explains the fact that no single base frequency was found in this low turbulence flow. Probably, a single value base turbulence frequency can exist if the horizontal wall is adiabatic or isothermal and can allow the turbulence to be totally damped along the wall. This is not the case in this study.

3.3. The probability density function (PDF)

The PDF method is a very useful tool for analysing random processes and is currently used extensively in the study of turbulent combustion (Kuzenetsov and Sabel'nikov [20]). Spalding [21] developed a multi-fluid model (MFM) of turbulence. When 'multi' becomes a large number, it can be truly said that the MFM is just another form of a PDF-transport model. Therefore, direct knowledge of the PDF of low turbulent natural convection in cavities is useful for the validation of CFD codes based on the PDF method. The turbulent quantities should be in the Gaussian distribution if the fluid flow is a homogeneous turbulence flow. Probability density functions T', u' and v' at $Y = 0.5$ are shown in Fig. 6. Fig. 6(a) shows the PDF of T' having a peak on the positive side. The distribution of u' and v' is different from each other. This indicates again that the two components fluctuate randomly and do not correspond to each other. At this point ($X = 0.9859$), the PDF of u' (Fig. 6(b)), is nearly symmetrical but the PDF of v' (Fig. 6(c)), is similar to T' having a peak on the positive side. The asymmetrical distribution indicates that the flow is not homogeneous.

The skewness (S) and flatness (F) factors defined below can be used to determine if a discrete random variable x is in a Gaussian distribution or not.

$$S = \frac{\overline{(x-\bar{x})^3}}{\left(\overline{(x-\bar{x})^2}\right)^{3/2}} \tag{1}$$

$$F = \frac{\overline{(x-\bar{x})^4}}{\left(\overline{(x-\bar{x})^2}\right)^{2}} \tag{2}$$

The skewness gives a measure of the symmetry of the probability distribution of the random variable, i.e. the skewness is zero for a perfectly symmetric distribution. The flatness gives a measure of how fast the probability distribution goes to zero. If S and F have values of 0 and 3, respectively, the variable is in Gaussian distribution (McComb [22]).

The skewness and the flatness of T' at mid-height was calculated and shown in Fig. 7. S and F are near 0 and 3, respectively in the core area but differ from these values in the boundary layer. The skewness has a value of about 1 at the cold wall then decreases to about -2 at $X = 0.975$. From this point, S is increasing until $X \approx 0.915$ then decreases rapidly to about 0. The flatness is more varied than the skewness. It has a value of about 4 at the cold wall then decreases to about 2 at $X = 0.993$. From this point, it rises up to a peak of 12 at $X \approx 0.975$. Then its value drops to about 3.5 at $X \approx 0.96$ and rises up to about 15 at $X \approx 0.915$. From there it drops again to about 3. The skewness and flatness of the velocity fluctuation are also shown in Fig. 7. Similar to the temperature fluctuation, from $X = 0.9$ to the cavity centre S and F have the value of about 0 and 3, respectively, i.e. u' and v' are in Gaussian distribution. However, in the boundary layer S and F vary significantly. S and F of both velocity components have two peaks, one near the wall and the other in the boundary layer. In the inner layer of the boundary (between wall and velocity peak point about $0.99 < 1$) S and F values are close to 0 and 3, respect-

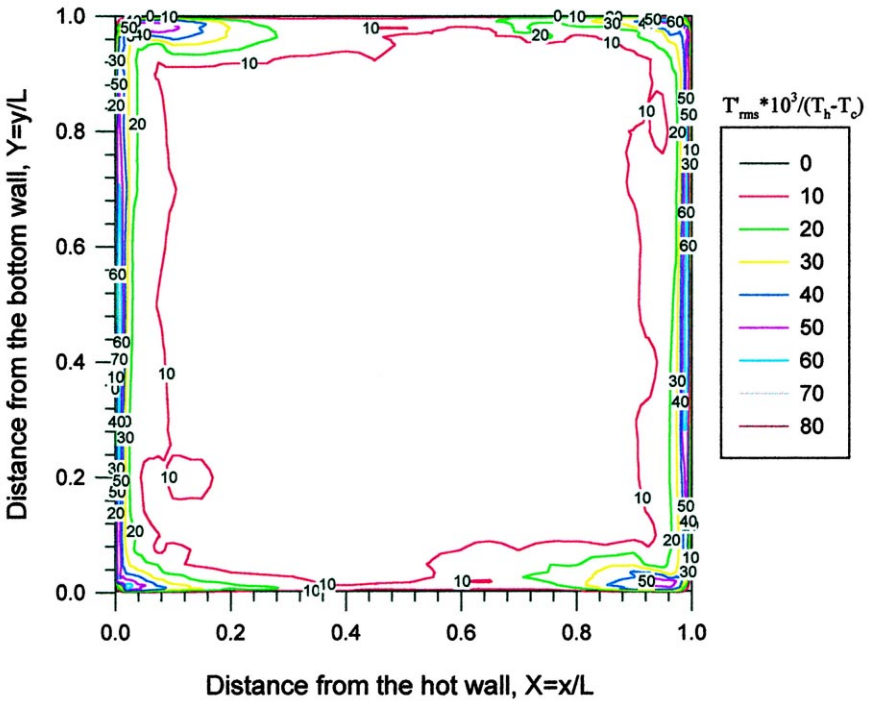

Fig. 9. Contour plot of temperature fluctuation $(T'_{\mathrm{rms}})/(T_{\mathrm{h}}-T_{\mathrm{c}})\times 10^3$.

ively. In the outer layer of the boundary (from the velocity peak point to the outer edge of the boundary, about $0.9 < 0.99$), the values of S and F differ significantly from 0 and 3. The skewness of u' can be down to -2.3 and the flatness can be up to 16.7; S of v' can be down to -1.7 and F can be up to 7.5. Hence, in the boundary layer the velocity fluctuation is not in the Gaussian distribution. In conclusion, there is no simple PDF distribution for the temperature and velocity fluctuations in the cavity.

3.4. The root mean square of the fluctuation quantities

In turbulent flow, both the time average and fluctuation parameters are important in describing the flow and as mentioned in Section 1, turbulence modelling requires equations relating to the fluctuation parameters in addition to the basic governing equations. The rms results of the temperature fluctuation for different heights are shown in Fig. 8. A constant has been added to each successive group data to avoid overlap. As seen in the figure, the temperature fluctuation intensity increases with distance from the wall to a peak and then decreases to almost nothing. At mid-height the T'_{rms} distribution is symmetrical and has a maximum value of $T'_{\mathrm{rms}} = 3.0$ K $(T'_{\mathrm{rms}}/(T_{\mathrm{h}}-T_{\mathrm{c}}) = 0.075)$ near both the hot and cold walls. In general, the temperature fluctuation distribution in the cavity is nearly anti-symmetrical about the cavity centre. The very slight deviation from complete anti-symmetry is possibly due to changes in fluid properties. In numerical work, the Boussinesq assumption is valid when the temperature difference is less than 28.6 K in an air filled cavity [23]. According to Gifford [24], the anti-symmetrical feature disappears in non-Boussinesq solutions. In our experiments the temperature difference was 40 K. Numerical modelling and comparison with the data will be useful to clarify the effect of this higher temperature difference on symmetry. Fig. 9 is a contour plot of the non-dimensional temperature fluctuations in the cavity mid-plane confirming the above points. It can also be seen clearly that the temperature fluctuation is mostly concentrated in the area near the isothermal walls (from the wall to about $0.1L$). In addition, the core area is stationary with no temperature fluctuation at all. The recorded 0.1 K value in the core is mainly due to the noise [18].

The experimental results of u'_{rms} and v'_{rms} at different heights are shown in Fig. 10. Again a constant was added to clarify the presentation and $V_0 = 1$ m/s. The velocity fluctuations are concentrated in the boundary layer and decrease to almost nothing outside the boundary layer. As with the temperature, the small recorded value in the core area is caused by noise. One

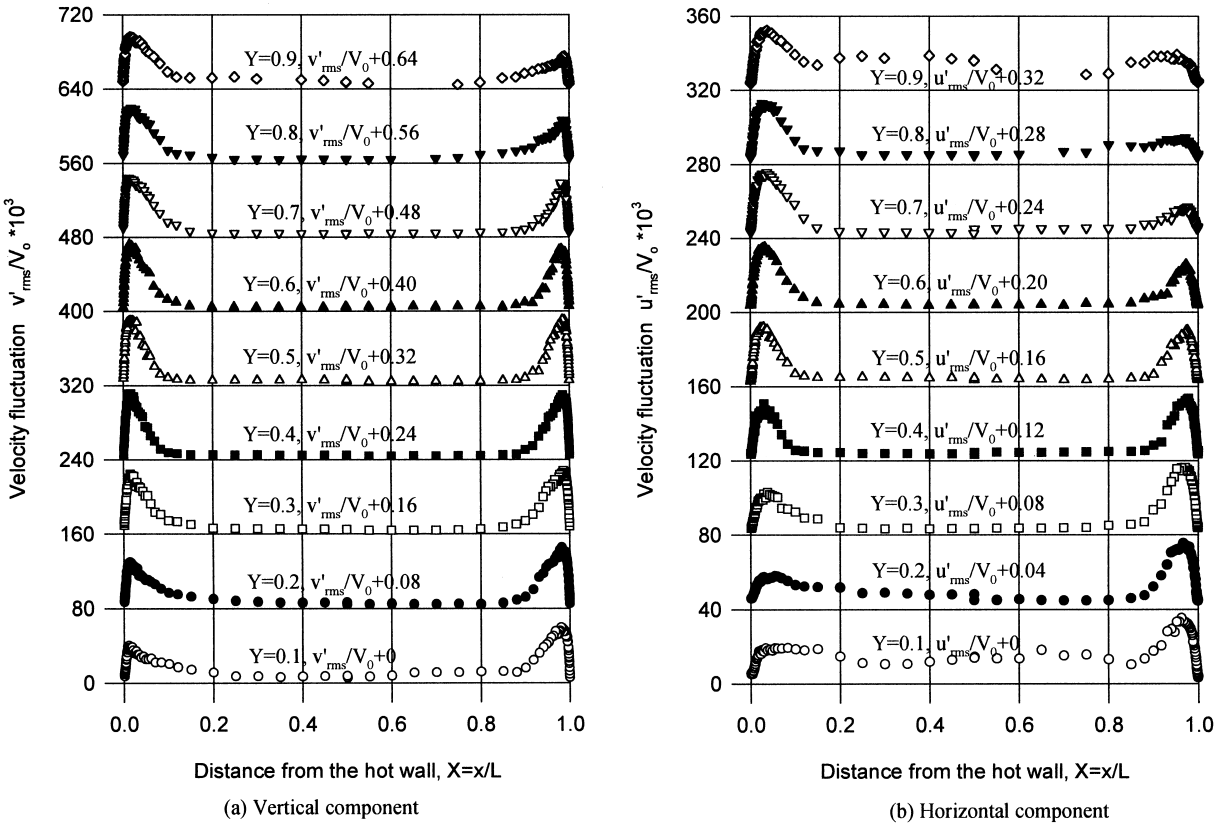

Fig. 10. Velocity fluctuation at different heights.

feature shown in Fig. 10 is the difference between u'_{rms} and v'_{rms}. The value of u'_{rms} is less than half that of v'_{rms} in the boundary layer at the cavity mid-height. The distributions of v'_{rms} and u'_{rms} based on all of the experimental measurements are shown in Figs. 11 and 12, respectively. The distribution of fluctuation quantities is basically anti-symmetric. In vertical cavities boundary layer flow is expected at the active walls. Heat transfer at the horizontal walls creates boundary layer flow on these walls as well. The change in the flow direction as the fluid flow meets the vertical walls causes some low turbulence in the corner regions. Velocity fluctuation is detected everywhere along the walls, with the vertical fluctuation dominating near the isothermal walls. The horizontal velocity fluctuation is prominent near the top hot corner and the bottom cold corner.

In turbulence modelling, one important hypothesis is isotropy [25]. For natural convection in cavities, the flow must be anisotropic particularly close to solid boundaries since the flow is limited near the solid walls. On the wall, the velocity and its fluctuation equal to zero. The flow reaches the strongest anisotropic point at the middle of the viscous layer ($\Delta X \approx 0.002$ from the wall, $v'_{rms}/u'_{rms} = 5$). Outside the viscous layer, the level of the anisotropy decreases across the boundary layer. In the core area, the fluid is stationary; no velocity and no fluctuation. This structure should be considered by numerical modellers.

In this deep cavity ($Ar_z = 2$), the flow is two-dimensional at the mid-section. This means that $\bar{w} = 0$. Cebeci and Bradshaw [26] reported that in isotropic turbulent flow, w' is of the same order as u' and v' even if $\bar{w} = 0$. In this anisotropic turbulent natural convection, it is very difficult to estimate w' without direct measurements. Experimental and numerical evidence by Kreplin and Eckelmann [27] and Spalart [28], respectively suggest that along an isothermal vertical wall:

$$\overline{u'^2} \leq \overline{w'^2} \leq \overline{v'^2} \tag{3}$$

As a first estimation, we can use

$$\overline{w'^2} = \frac{\overline{u'^2} + \overline{v'^2}}{2} \tag{4}$$

i.e. the turbulent fluctuation in the z-direction contributes one third of the turbulent kinetic energy (k).

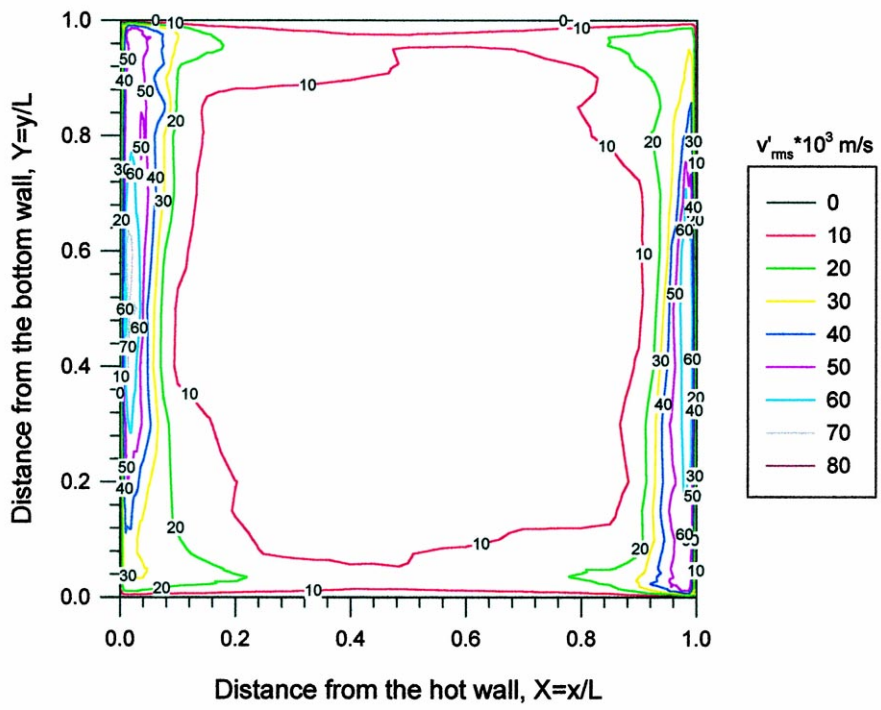

Fig. 11. Contour plot of the vertical velocity fluctuation, $v'_{rms} \times 10^3$ m/s.

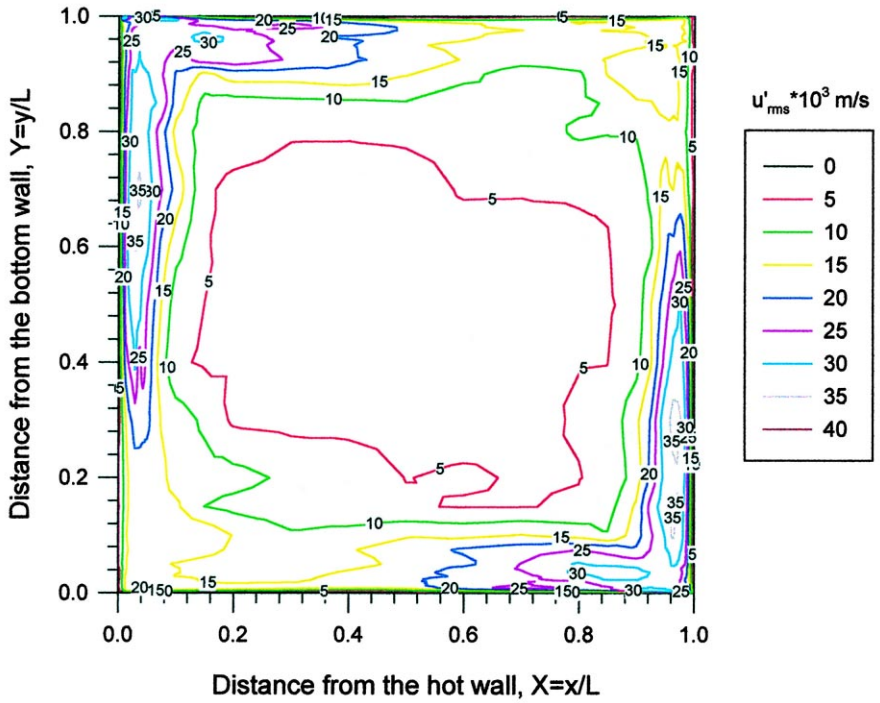

Fig. 12. Contour plot of the horizontal velocity fluctuation, $u'_{rms} \times 10^3$ m/s.

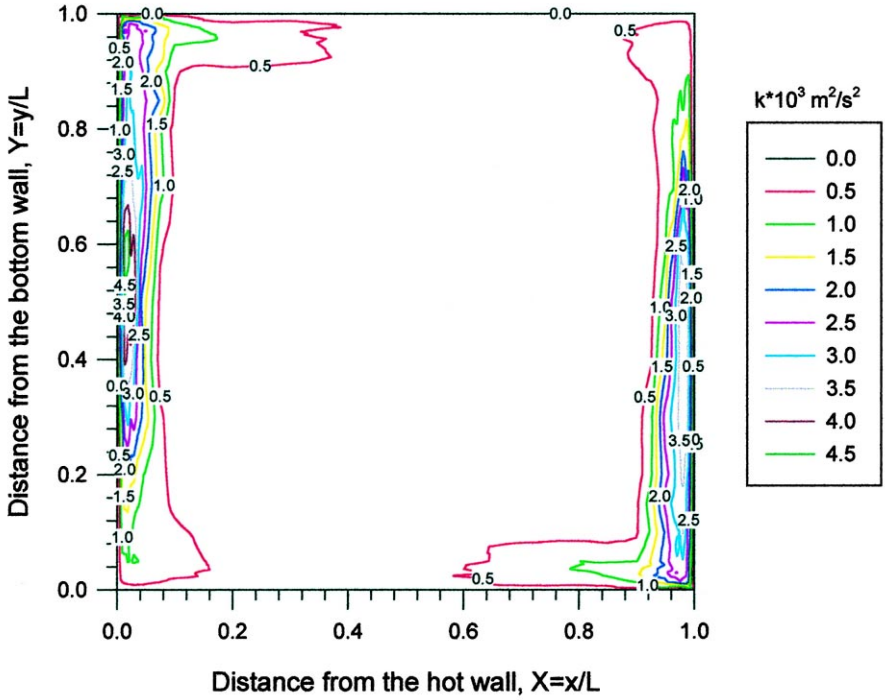

Fig. 13. Distribution of the estimated turbulent kinetic energy, $k \times 10^3$ m^2/s^2.

Therefore,

$$k = \frac{1.5(\overline{u'^2} + \overline{v'^2})}{2} \tag{5}$$

The mean velocity both in the x- and y-directions was measured using LDA with BSA with an accuracy of 0.07% [18,29]. In this work, the flow parameters near the walls are of particular interest. The experimental results near the walls were a statistical average of 20,000 readings at each point so that their error was negligible. If the estimated $\overline{w'^2}$ has an accuracy of 20%, the estimated turbulent kinetic energy will be true with an accuracy better than 4% ($\overline{w'^2}$ contributes only one third to k).

The experimental results based on Eq. (5) are shown in Fig. 13. They clearly indicate that the turbulence flow is limited in the boundary layer and its intensity increases along the flow direction until the horizontal walls are experienced by the flow. Comparing Fig. 9 with Fig. 13, the estimated distribution of turbulent kinetic energy is different from the distribution of the temperature fluctuation. The later one has nearly the same intensity at the lower part of the hot wall (and the upper part of the cold wall) as at mid-height. This confirms that the velocity fluctuation is not coincident with the temperature fluctuation.

The Reynolds time average equations include the Reynolds stress, $-\rho\overline{u'v'}$. The air density in this term is

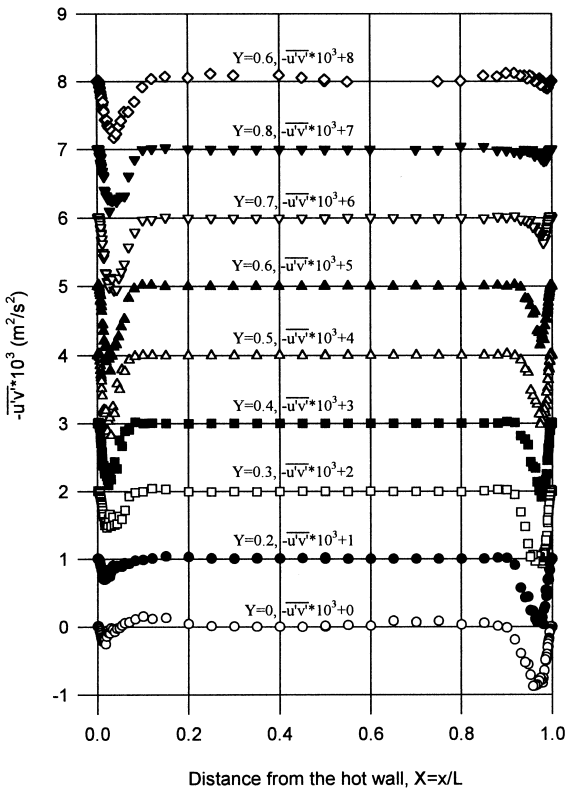

Fig. 14. Distribution of Reynolds stress at different heights.

based on the mean temperature distribution which is measured separately. In this study, the turbulent fluctuation quantity $\overline{u'v'}$ was directly measured by the two dimensional LDA with BSA. The results at different heights are shown in Fig. 14. At mid-height the values of $-\overline{u'v'}$ near the two walls differ by about 10%. Since the 40 K temperature difference causes about an 11% density difference in the cavity, the distribution of the Reynolds stress at mid-height is then symmetric. In particular, for the first 3 mm from the active walls, $-\overline{u'v'}$ is near zero. Then it decreases rapidly to a negative peak of about -1.1×10^{-3} m^2/s^2 (-1.0×10^{-3} m^2/s^2 near the cold wall side). The peak is located outside the velocity peak at about 15–21 mm from the wall. $-\overline{u'v'}$ is near zero between $X = 0.1$ and 0.9 at mid-height. The distribution of $-\overline{u'v'}$ changes significantly with height along the active hot wall. At the hot bottom corner, $-\overline{u'v'}$ shows two peaks along the horizontal axis; a negative of -0.23×10^{-3} m^2/s^2 and a positive of 0.17×10^{-3} m^2/s^2. The absolute value of the negative peak increases with increasing distance from the bottom wall until about mid-height. Following that, the peak value decreases slightly with increasing distance from the bottom wall. On the other hand, the positive peak decreases monotonically with increasing distance from the bottom and at mid-height it nearly disappears. Similar variations exist at the cold wall. A contour plot of Reynolds stress (in this case $-\overline{u'v'}$) is shown in Fig. 15 based on all the experimental data and indicates the anti-symmetric nature of the distribution. As also seen earlier, the turbulence is more intense near the active walls than anywhere else. The Reynolds stress is generally limited downstream of the boundary layers on the hot and cold walls indicating the development of turbulence in the flow.

4. Comparison and discussion

The fluid flow in the cavity is a low turbulence wall shear flow. The fluctuations of the temperature and the two velocity components are independent. The frequency of the fluctuation is dependent on the location and it increases along the direction of flow on the isothermal walls. A low frequency range (0.1–0.2 Hz) rather than a single value base frequency is evident in our experiments. This is caused by the horizontal walls; the highly conducting horizontal walls damp only partially the turbulence. Fluctuation is limited in the boundary layer along the walls and in the core area the fluid is stationary so there is no fluctuation at all in this region. King [13] and Mergui and Penot [16] reported turbulent fluctuation in the core of the cavity. This was possibly the result of heat losses which cause more intense turbulence, three dimensional flow and stronger asymmetry. In numerical studies, Genhard and Mahajan [30] reported a characteristic frequency about 0.35 Hz for vertical air free convection. For natural convection in cavities, Henkes and Hoogendoorn [31] indicated that the conductivity of the horizontal wall decreases the flow stability. The non-dimensional frequency of the oscillation, $fH/\sqrt{g\beta\Delta TH}$, was about 0.25 for the ideal perfectly conducting horizontal wall and was almost independent of the Rayleigh number. The corresponding dimensional frequency for the present study is about 0.33 Hz. The lower value obtained in our experiments (0.1–0.2 Hz) is possibly due to the fact that the horizontal walls are highly conducting rather than perfectly conducting. If the real experimental conditions are included, a numerical model should be able to predict closer the experimental findings.

As discussed in Part I [1], the thermal and momentum boundary layers of turbulent natural convection can be characterised by a two layer structure, namely an inner layer (including a viscous/conductive layer and a buoyant sub-layer) and an outer region [2,5]. Directly against the vertical wall, there are the conductive and viscous layers, where the temperature is nearly linear and the velocity profile is cubic. At mid-height, the thickness of the conductive layer (3 mm) was called by George and Capp [2] as the thermo-visous layer. The distribution and relation between the fluctuation quantities near the wall are shown in Fig. 16. The Reynolds stress is nearly zero in the conductive layer (in fact, it is zero up to 4 mm from wall) but T'_{rms}, v'_{rms} and u'_{rms} vary significantly. In the outer layer, the viscous and conduction terms are negligible. No direct relation was found between the Reynolds stress and the mean velocity. However, the Reynolds stress is nearly zero in the thermo-viscous layer, increases rapidly in the buoyant sub-layer and reaches its maximum in the outer region. The peak is coincident with the turbulent kinetic peak but independent of the temperature fluctuation.

Very limited data on the fluctuation quantities have been reported in the past in either experimental or numerical studies, especially for square cavities. The few results found in literature are at mid-height. The temperature fluctuation results at mid-height are compared in Fig. 17. The results of King [13] and Ziai [14] for the high cavity ($Ar_x = 5$) suffered heat losses, which caused asymmetrical distribution, a higher turbulence and three dimensional flow. The thermal boundary layer in this high cavity is much thicker than that in the present square cavity. The experimental results are also compared with the direct numerical simulation results of Paolucci [5]. The numerical results were based on an air filled square cavity at $Ra = 10^{10}$. There is better agreement with the present results than those of [13,14] for a high cavity. The small difference between the present results and results of Paolucci [5]

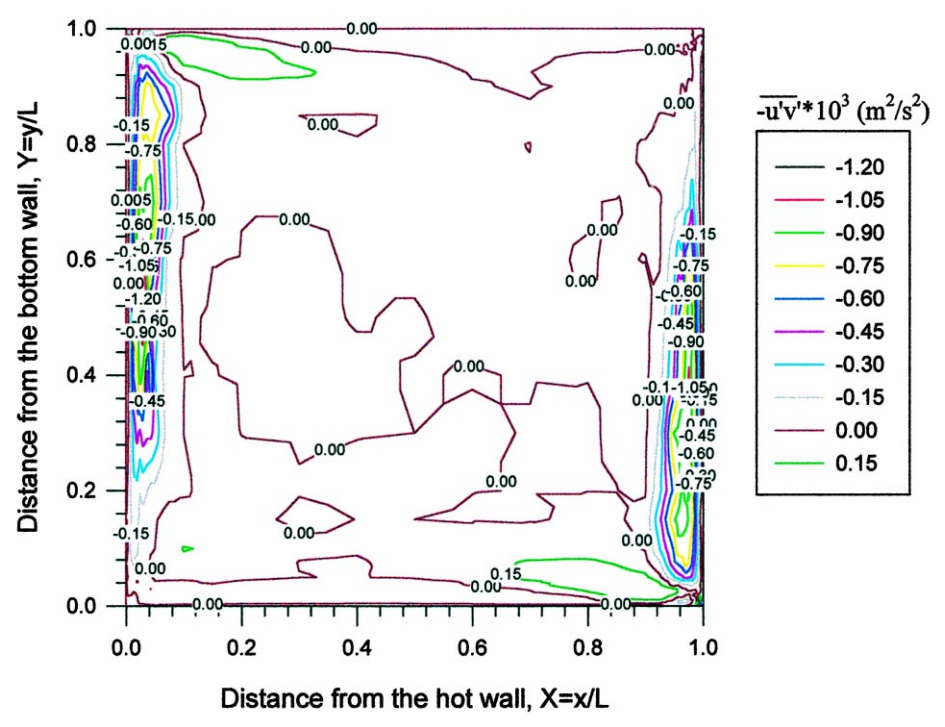

Fig. 15. Contour plot of the distribution of the Reynolds stress.

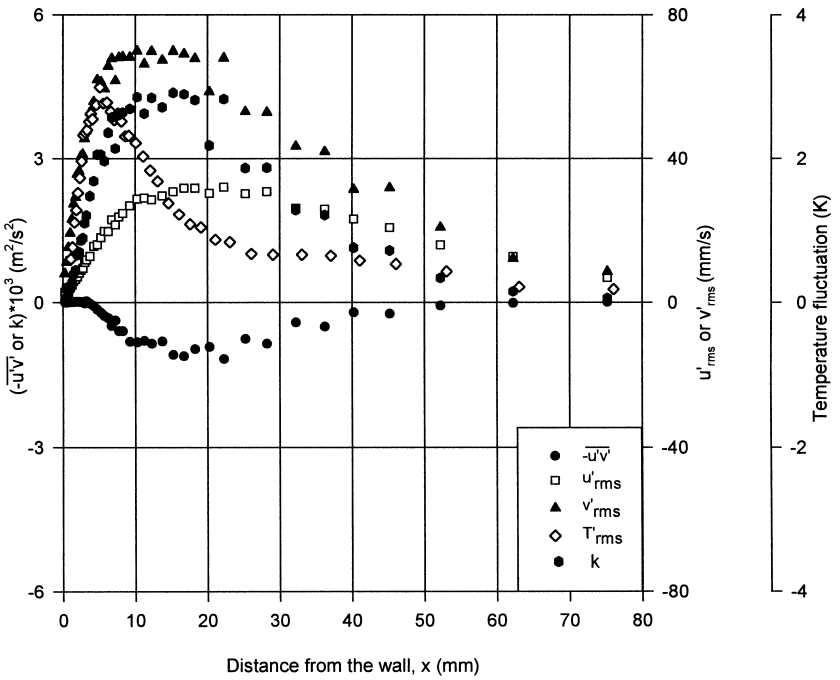

Fig. 16. Relation between turbulent fluctuation quantities near the hot wall at $Y = 0.5$.

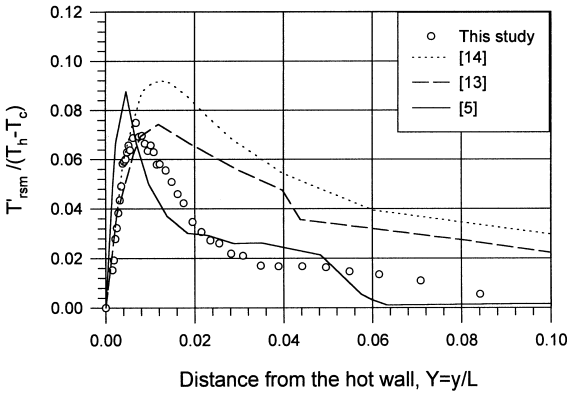

Fig. 17. Comparison of the temperature fluctuation near the hot wall at $Y = 0.5$. This study $Ra = 1.58 \times 10^9$, $Ar_x = 1$; [14] $Ra = 5 \times 10^8$, $Ar_x = 6$; [13] $Ra = 3.53 \times 10^8$, $Ar_x = 5$ and [5] $Ra = 10^{10}$, $Ar_x = 1$.

is possibly caused by differences in the Rayleigh number (10^{10}) and boundary conditions at the horizontal walls. In the numerical simulation, the horizontal walls were assumed to be adiabatic.

In Fig. 18 the vertical velocity fluctuation results of the present study are compared with the direct numerical simulation results of Paolucci [5] and the experimental results of Lankhorst [15]. The high Ra number results ($Ra = 2.1 \times 10^9$) of [15] are in general agreement with the present results. However, they are higher than the present values at $X > 0.05$ and carry a larger scatter. The vertical velocity fluctuation very close to

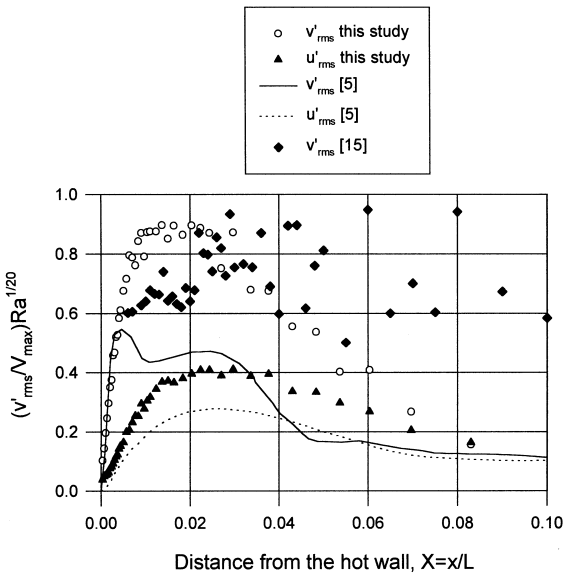

Fig. 18. Comparison of the velocity fluctuation at mid-height. This study $Ra = 1.58 \times 10^9$, [5] $Ra = 10^{10}$, [15] $Ra = 2.1 \times 10^9$.

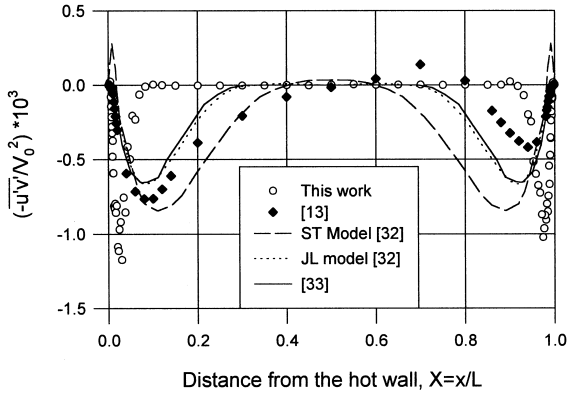

Fig. 19. Comparison of Reynolds stress with eariler results obtained at $Ra = 2.824 \times 10^8$, $Ar_x = 5$ (ST: standard, JL: Jone-Launder).

the hot wall given by [5] for a square cavity at $Ra = 10^{10}$ is in good agreement with the present results. However, the predicated value of the maximum vertical velocity fluctuation is only half as large as the present measured results. The horizontal velocity fluctuation is of similar distribution but only two third as large as the present measured values. The lower predicted value is possibly due to the effect of the horizontal boundary. At the same Ra number, the turbulence intensity in a cavity with adiabatic horizontal walls is lower than that in a cavity with perfectly conducting walls. The double peak structure in the vertical velocity fluctuation seen in the results of [5] was not present in the current measurements. His second vertical component peak is coincident with the peak in the horizontal component. No explanation had been given for this double peak structure.

Only few experimental results of Reynolds stress were reported in the past. The results of King [13] were strongly asymmetric and Mergui and Penot [16] gave much smaller values. The reason is not clear. King [13] did not directly measure the Reynolds stress in his experiments. He used an integral equation to calculate the Reynolds stress from the measured time average data of temperatures and velocities. As reported by King [13], discrepancies were found along the centre-line from the hot to the cold wall. From comparison in Fig. 19, it can be seen that the agreement between the present results and those of [13] is good in the near wall area. The difference increases with increasing distance from the wall. King [13] reported a non-zero value in the core while the present data are nearly zero between $X = 0.1$ and 0.9. To date, many numerical modelling results were obtained for $Ra = 4 \times 10^8$ and $Ar_x = 5$, because Cheesewright and his team of researchers [10–14] produced a set of experimental data for these values of Ra and Ar_x. A

comparison is made in Fig. 19 with Henkes and Hoogendoorn [32] and Ince et al. [33]. The results obtained by King [13] are not in good agreement with the numerical results and it is difficult to state which of the two — experimental results by King [13] or numerical results by Henkes et al. and Ince et al. [32,33] is more reliable. The present results are not directly comparable due to differences in Ra and Ar_x. They are in the low turbulence region and the boundary layer is much thinner than that in the high cavity of $Ar_x = 5$. The Reynolds stress predicted by the standard k–ε model [32] shows a positive peak near the wall. This peak was not found in the present experimental and other numerical modelling results. Future numerical modelling under the present experimental conditions will help elucidate this point and others and improve modelling techniques. As mentioned before, such modelling should include realistic temperature and heat flux values at the top and bottom walls of the cavity given in Part I [1].

5. Conclusions

An experimental study of two-dimensional low turbulence natural convection in an air filled vertical square cavity was conducted at a Ra number of 1.58×10^9. The fluid flow in the cavity was turbulent. Its fluctuating thermal and momentum field were systematically surveyed. The temperature and the velocity components fluctuated independently and were limited in a boundary layer along the solid wall. The flow was in the low turbulence region with a base frequency in the range 0.1–0.2 Hz. The frequency increased with flow direction along the isothermal walls. In the core region, the fluid was stationary; no mean flow and no fluctuation. The fluctuations varied across the cavity and in the boundary layer they were not in Gaussian distribution. The experimental results of T'_{rms}, u'_{rms}, v'_{rms} and Reynolds stress are reported for the first time in contour plots. Differences with earlier reported results were obvious. Further studies with the boundary conditions of the present results are strongly encouraged to assist in elucidating some of the differences obtained in this comparison between the experimental and the numerical results. Such work will contribute to the efforts to improve CFD modelling.

References

[1] Y.S. Tian, T.G. Karayiannis, Low turbulence natural convection in an air filled square cavity Part I: the thermal and fluid flow fields, Int. J. Heat Mass Transfer, 43 (2000) 849–866.

[2] W.K. George, S.P. Capp, A theory for natural convection turbulent boundary layer next to heated vertical surfaces, Int. J. Heat Mass Transfer 22 (1979) 813–826.

[3] K. Hanjalic, S. Vasic, Computation of turbulent natural convection in rectangular enclosures with an algebraic flux model, Int. J. Heat Mass Transfer 36 (1993) 3603–3624.

[4] F.T.M. Nieuwstadt, Direct and large-eddy simulation of free convection, Proc, in: 9th Heat Transfer Conf., Jerusalem, Israel, vol. 1, 1990, pp. 37–48.

[5] S. Paolucci, Direct numerical simulation of two-dimensional turbulent natural convection in an enclosed cavity, J. Fluid Mech 215 (1990) 229–262.

[6] P.L. Betts, A.A. Dafa'Alla, Turbulent buoyant air flow in a tall rectangular cavity, Winter Annular of ASME HTD-60 (1986) 83–92.

[7] P.L. Betts, I.H. Bokhari, New experiments on turbulent natural convection of air in a tall cavity, in: Proc. 4th UK Heat Transfer Conference, 1995, pp. 213–216.

[8] P.W. Giel, F.W. Schmidt, An experimental study of high Rayleigh number natural convection in an enclosure, in: Proc. 8th. Int. Heat Transfer Conf., San Francisco, USA, vol. 4, 1986, pp. 1459–1464.

[9] P.W. Giel, F.W. Schmidt, A comparison of turbulence modelling predictions to experimental measurements for high Rayleigh number natural convection in enclosures, in: Proc. 9th. Int. Heat Transfer Conf., Jerusalem, Israel, vol. 2, 1990, pp. 175–180.

[10] R. Cheesewright, K.J. King, S. Ziai, Experimental data for the validation of computer codes for the prediction of two-dimensional buoyant cavity flows, Winter Annual Meeting of ASME HTD-60 (1986) 75–82.

[11] R. Cheesewright, S. Ziai, Distributions of temperature and local heat-transfer rate in turbulent natural convection in a large rectangular cavity, in: Proc. 8th. Int. Heat Transfer Conf., San Francisco, USA, 1986, pp. 1465–1470.

[12] R. Cheesewright, K.J. King, Stress distributions in turbulent natural convection in a rectangular air cavity, in: Proc. 9th. Int. Heat Transfer Conf., Jerusalem, Israel, vol. 2, 1990, pp. 161–167.

[13] K.J. King, Turbulent natural convection in rectangular air cavities, PhD thesis, Queen Mary and Westfield College, University of London, London, UK, 1989.

[14] S. Ziai, Turbulent natural convection in a large rectangular air cavity, PhD thesis, Queen Mary and Westfield College, University of London, London, UK, 1983.

[15] A. M. Lankhorst, Laminar and turbulent natural convection in cavities: numerical modelling and experimental validation, PhD thesis, Technology University of Delft, Netherlands, 1991.

[16] S. Mergui, F. Penot, Natural convection in a differentially heated square cavity: experimental investigation at $Ra = 1.69 \times 10^9$, Int. J. Heat Mass Transfer 39 (1996) 563–574.

[17] Y.S. Tian, T.G. Karayiannis, R.D. Matthews, Velocity measurement in low turbulence natural convection using two-dimensional LDA with BSA, IMechE Conf. Trans. 1998-2, Optical Methods and Data Processing in Heat and Fluid Flow, 1998, pp. 65–73.

[18] Y.S. Tian, Low turbulence natural convection in an air

filled square cavity, PhD thesis, South Bank University, London, UK, 1997.
[19] K.T. Yang, Transitions and bifurcations in laminar buoyant flows in confined enclosures, Trans. ASME, Journal of Heat Transfer 110 (1988) 1191–1204.
[20] V.R. Kuzenetsov, V.A. Sabel'nikov, Turbulence and Combustion, Hemisphere, Washington, DC, 1990.
[21] D.B. Spalding, The plane turbulent mixing layer, simulated by a multi-fluid model of turbulence, in: Proc. of 5th UK National Conf. on Heat Transfer, Session G, London, 1997.
[22] W.D. McComb, The Physics of Fluid Turbulence, Oxford University Press, Oxford, London, 1996, p. 531.
[23] D.D. Gray, A. Giorgini, The validity of the Boussinesq approximation for liquids and gases, Int. J. Heat Mass Transfer 19 (1976) 545–551.
[24] W.A. Gifford, Natural convection in a square cavity without the Boussinesq approximation, 49th Annual Technical Conference-ANTEC '91, 1991, pp. 2448–2454.
[25] M.M. Stanisic, The Mathematical Theory of Turbulence, 2nd ed, Springer–Verlag, Berlin, 1998.
[26] T. Cebeci, P. Bradshaw, Physical and Computational Aspects of Convective Heat Transfer, Springer–Verlag, Berlin, 1988.
[27] H.P. Kreplin, H. Eckelmann, Behaviour of the three fluctuating velocity components in the wall region of a turbulent channel flow, Phys. Fluids 22 (1979) 1233–1239.
[28] P.R. Spalart, Direct simulation of a turbulent boundary layer up to $R_\theta = 1410$, J. Fluid Mech 187 (1988) 61–98.
[29] J.F.M. Maybrey, Mean velocity calibration comparison of a laser Doppler anemometer, Dantec Information, No. 13, 1994, pp. 10–13.
[30] B. Gebhart, R. Mahajan, Characteristic disturbance frequency in vertical natural convection flow, Int. J. Heat Mass Transfer 18 (1975) 1143–1148.
[31] R.A.W.M. Henkes, C.J. Hoogendoorn, Bifurcation to unsteady natural convection for air and water in a cavity heated from the side, in: Proc. 9th Int. Heat Transfer Conf. Jerusalem, Israel, vol. 2, 1990, pp. 257–262.
[32] R.A.W.M. Henkes, C.J. Hoogendoorn, Turbulent natural convection in enclosures, in: R.A.W.M. Henkes, C.J. Hoogendoorn (Eds.), Turbulent Natural Convection In Enclosures: A Computational And Experimental Benchmark Study, Europeennes Thermique et Industrie, 1993, pp. 64–75.
[33] N.Z. Ince, P.L. Betts, B.E. Launder, Low Reynolds number modelling of turbulent buoyant cavity flows, in: R.A.W.M. Henkes, C.J. Hoogendoorn (Eds.), Turbulent Natural Convection in Enclosures — A Computational and Experimental Benchmark Study, Europeennes Thermique et Industrie, 1993, pp. 76–87.